5 Soft-matter Project

Project Leader: Hideki Seto

5-1 Introduction

Soft-matter is a subfield of condensed matter comprising a variety of physical states that are easily deformed by thermal stresses or thermal fluctuations. They include liquids, colloids, polymers, liquid crystals, amphiphilic molecules, and a number of biological materials. These materials often self-organize into mesoscopic physical structures that are much larger than the microscopic scale (the arrangement of atoms and molecules), and yet are much smaller than the macroscopic scale of the material. The properties and interactions of these mesoscopic structures may determine the macroscopic behavior of the material. In spite of the various forms of these materials, many of their properties have common physicochemical origins, such as a large number of internal degrees of freedom, weak interactions between structural elements, and a delicate balance between entropic and enthalpic contributions to the free energy. These properties lead to large thermal fluctuations, a wide variety of forms, sensitivity of equilibrium structures to external conditions, macroscopic softness, and metastable states.

We are investigating the structural properties of soft-matter such as liquids and amphiphilic molecules. Especially, structures formed under far-from-equilibrium conditions are interesting. These investigations will yield basic knowledge to help to solve the mystery of life.

5-2 Formation of a multiscale aggregate structure through spontaneous blebbing of an interface

The production and destruction of elastic material are key factors in cellular motion. For example, while a cell is moving, globular actin is transformed into a gel of filament actin and vice versa. The rate of production/destruction of the actin gel is controlled through information processing in a complex network of genetic materials such as DNA, RNA, and protein. In addition, the physical nature of the elastic material, especially its chemomechanical coupling and the resulting pattern formation, should also control the macroscopic behavior of cells. Furthermore, such pattern formation should be an essential mechanism leading to macroscopic dynamical order. In order to confirm these hypotheses, construction of a model system can help us to understand such physicochemical aspects of cellular motion by allowing us to detour the entangled feedback systems inherent in biology.

In this spirit, we recently constructed a system in which an elastic material is continuously produced at a deformable interface. The system consists of an aqueous phase with a cationic surfactant and an organic phase with a cosurfactant. In this system, a surfactant aggregate is formed at the oil–water interface and the aggregate subsequently disperses in the aqueous phase. The aggregate has a lamellar structure composed of surfactant, cosurfactant and water with a large interlayer distance of around a few tens of nanometers.

When the organic phase is deposited to float on the aqueous phase as a droplet, the interface between these two phases deforms locally and repeatedly. The shape of the local interfacial deformation is always circular, and hence we call this deformation as “bleb”. The circular shape of the bleb indicates that the bleb is caused by the increase in the internal pressure in the droplet (the organic phase). A single bleb slowly expands (~1 mm/s) and quickly contracts (~10 mm/s). These blebs appear at purely random positions and timings without any correlation between them. We call the process of bleb formation as “blebbing”. Blebbing is also seen in cellular membranes, and several studies suggest its relevance to cellular motility. To simulate the mechanism of blebbing, we have constructed a mathematical model based on the permeability, elasticity, and fragility of the aggregate. As the aggregate has permeability, surfactant can go through the aggregate, resulting in a constant supply of surfactant to the interface. Then, the aggregate is continuously formed at the interface. Gradually, the aggregate is pushed out by newly formed aggregate. The aggregate is stretched as it is pushed out, and the resulting stress from the elasticity of the aggregates squeezes a droplet. Thus, the pressure inside the droplet increases. At the same time, since the aggregate is fragile, it starts to collapse when the stress within it exceeds a certain critical value. This local collapse of the aggregate leads to the failure of homogeneous squeezing of the droplet. Consequently, the interface where the aggregate is collapsed starts to extrude. This is a short summary of the mechanism of interfacial blebbing. A mathematical model based on this conjecture correctly reproduced the relation between the size of a droplet and that of the blebs.

Although successful results have been obtained by using the above system, the dynamics in such a multi-scale system, especially the relation between microscopic dynamics (such as aggregate formation) and macroscopic dynamics (such as interfacial motion), remain unclear because there are no experiments that allow simultaneous observations of both microscopic and macroscopic behaviors. In order to answer the remaining questions concerning the interfacial motion

caused by aggregate formation, we constructed a quasi two-dimensional cell that had a thickness of 2 mm, as shown in Fig. 1(a).

Immediately after the organic phase and the aqueous phase came in contact with each other, the interface formed interfacial deformation, or bleb, continuously as previously reported in the case of a droplet. Some regions at the interface showed intensive blebbing, while others showed little. We call these two types of regions blebbing and non-blebbing regions. Lumps of aggregate, called "pillars", appeared in each non-blebbing region of the oil–water interface, and grew steadily from the oil–water interface downward to the aqueous phase, as seen in the snapshots in Fig. 1(b). The spatial periodicity of the blebbing and non-blebbing regions, which is the average pillar-to-pillar distance, was around 2.6 mm.

In a non-blebbing region, a pillar was generated and grew downwards from the oil–water interface. The length of the pillars, *l*, increased with time, while the width of the pillars did not. There was no significant

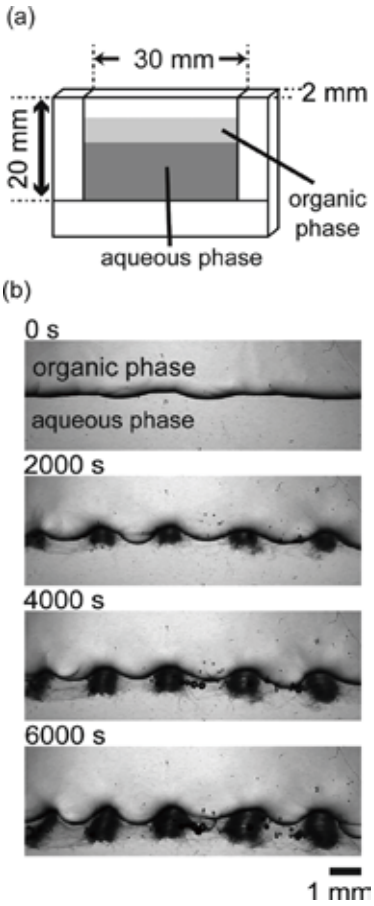

Fig. 1 (a) Sample cell for the micro-beam SAXS experiment. (b) Formation of a pillar-like structure of surfactant aggregates at the oil–water interface. Between the pillars, the oil–water interface exhibits intensive blebbing.

difference in the growth rate among the pillars. Figure 1(b) shows that the shape of a pillar around its tip (bottom) did not change as *l* increased, which implies that the formation of pillars occurred near the oil–water interface rather than around the pillar tip.

Micro-beam SAXS was performed at BL-4A in Photon Factory to determine the microscopic structure of the aggregate inside of a pillar while obtaining the position determined with 10-μm precision. Figure 2 shows the micro-beam SAXS results for a single pillar. As shown in Fig. 2(a), we scanned along a line approximately 1 mm below the interface and observed sharp Bragg peaks with twofold symmetry at the location of the pillar. From the symmetry of the scattering pattern, a microscopic structure of aggregate in the pillar is concluded to be a polarized lamella. All the observed peaks could be higher order peaks of the first Bragg peak hidden by a direct beam stopper, because the intervals between the peaks, Δq, are the same. Thus, we estimated a repeat distance of lamellae, d, to be 28–30 nm from the relation $d = 2\pi/\Delta q$. Furthermore, the orientation of the Bragg peaks depended on the measurement position in the pillar, which was parallel to the stacking direction of lamellae.

Figure 2(b) shows the spatial dependence of the total scattering intensity of the lamellae, I_t, and their orientation angle θ_p. I_t corresponds to the amount of regular structure at the beam spot in the aggregate. The direction of lamellae at the position is perpendicular to θ_p. The x axis is set horizontally, parallel to the averaged position of the oil–water interface. I_t is defined as the sum of the radial and angular scattering intensities; the orientation θ_p is defined as the angle of the maximum scattering intensity of the Bragg peaks. I_t showed small fluctuations with respect to x, indicating that the pillar was composed of a number of domains whose size should be comparable to the sum of the scanning step and the beam width, that is, about 25 μm. Inside of a domain, the stacking direction of lamellae was well ordered. We therefore consider the orientation of the domain which is parallel to the stacking direction of constituent lamellae. The orientation of the domain is strongly correlated with the position inside the pillar. The domain (and hence, the stacking direction of constituent lamellae) was horizontally oriented in the central part of the pillar, while the tilted one was observed at the edge of the pillar.

The dependence of the strength and orientation of scattering pattern on the position are shown in Figs. 2(c) and (d). Here we defined two values, $I_m(q, x)$ and $I_s(\theta, x)$; $I_m(q, x)$ is the maximum value of the scattering intensity at various azimuths θ for each q, and $I_s(\theta, x)$ is the integration of the scattering intensity over all wave

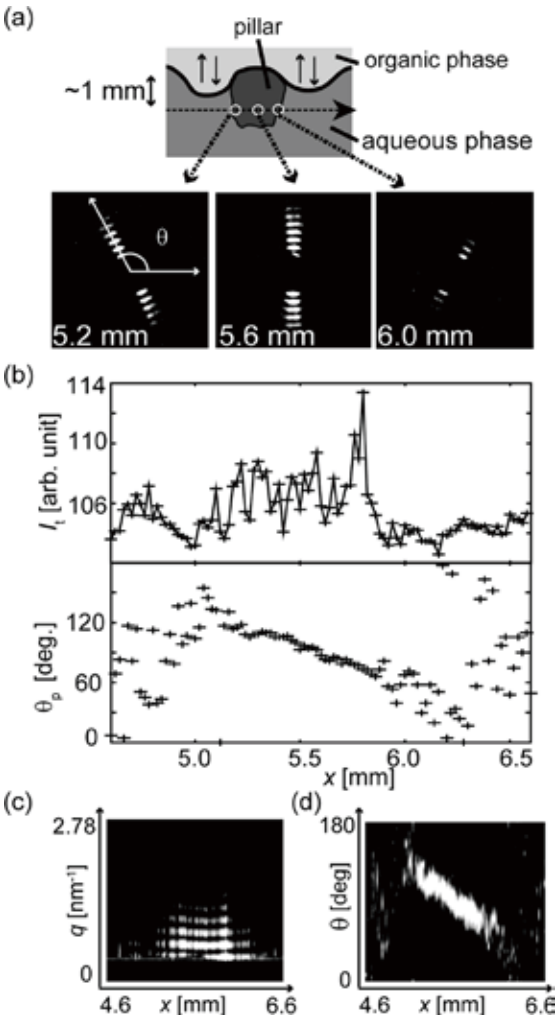

Fig. 2 (a) Schematics of the scanning of a single pillar with a micro-beam SAXS. Typical 2D images are shown related to the position in the lower three figures corresponding to those in (b). (b) Total scattering intensity It and the peak angle of scattering intensity are shown with respect to the scanning position x. (c) Plot of the angular maximum of the scattering intensity $I_m(q, x)$. Brighter color corresponds to larger $I_m(q, x)$. (d) Plot of the radial integral of the scattering intensity, $I_s(\theta, x)$. Brighter color corresponds to larger $I_s(\theta, x)$.

numbers (q) for each θ. Thus, a repeat distance of lamellae, d, at each position x can be inferred from $I_m(q, x)$ by inspecting the vertical periodicity of the pattern shown in Fig. 2(c). On the other hand, the direction of the domain can be obtained from the peak position of $I_s(\theta, x)$ at each position x. In Fig. 2(c), the value of $I_m(q, x)$ is shown as the brightness of the pixels, which depends on q and x. This shows that the scattering intensity was strong in the region 5.2 mm < x < 6.0 mm and that polarized lamellae were found over this position range, although both the scattering intensity and interlayer distance showed fluctuations, indicating the existence of domains.

In Fig. 2(d), the value of $I_s(\theta, x)$ is shown as the brightness of the pixels, which depends on θ and x. θ_p in Fig. 2(b) is effectively the angle corresponding to the maximum intensity over θ in Fig. 2(d). In the region of x with large $I_m(q, x)$, $I_s(\theta, x)$ has a strong peak at a certain θ, which indicates that the lamellae were well ordered, and the orientation of domain (the stacking direction of lamellae) is strongly correlated with the position.

We suggest that the regular spacing of the pillars, which has not been observed in the case of a circular oil droplet floating on an aqueous phase, can be explained by the constant size of blebbing at the oil−water interface. A detailed mathematical analysis of the relation between the interfacial motion and the hierarchical spatial structures should be carried out in a future study; however, it is interesting to note that these hierarchical spatial structures are formed in a wide range of scales (nm to mm) through dynamical interfacial behaviors out of equilibrium, without any external control.

References

Y. Sumino, et al., Phys. Rev. E, **76** (2007) 055202(R).
Y. Sumino, et al., J. Phys. Chem. B **113** (2009), 15709.
Y. Sumino, et al., Soft Matter, **7** (2011) 3204.
Y. Sumino, et al., Langmuir, **28** (2012) 3378.

5-3 Lipid-protein complexes at the air-water interface

Complexation of the zwitterionic lipid, dipalmitoyl-sn-glycero-3-phosphocholine (DPPC), and the protein, bovine serum albumin (BSA), at the air–water interface has been studied by surface pressure ( ) – mean molecular area (A) isotherms and X-ray reflectivity. Although BSA has an isoelectric point nearly at pH • 4.8, the possibility of complex formation with lipid molecules has been investigated from a low (•4.0) to high (•9.0) range of pH in the presence of divalent cation, Ca^{2+}, in the water subphase. Both the isotherm and reflectivity analysis show that the interaction of BSA with lipid monolayer takes place from the low to high subphase pH range, i.e., complexation occurs both below and above the isoelectric point. Only one layer of BSA forms below the lipid monolayer; probable reasons for the formation of such complex have been proposed.

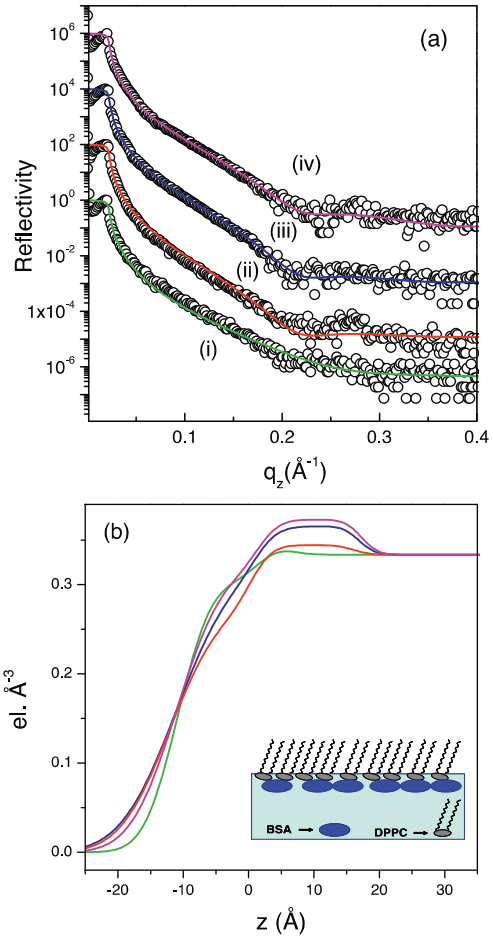

Fig. 3 (a) Specular X-ray reflectivity data (open circles) and analyzed curves (solid lines) as a function of qz for DPPC monolayer from (i) pure water subphase, (ii) water subphase containing 0.5 mg BSA, (ii) water subphase containing 0.5 mg/mL BSA, 5 mM $CaCl_2$ and at pH•7.1, (iv) water subphase containing 0.5 mg/mL BSA, 5 mM $CaCl_2$ and at pH•9. (b) Corresponding electron density profiles showing the average out-of-plane structure of the lipid-protein complexes.

References

S. Kundu, H. Matsuoka, and H. Seto, Colloids and Surf. B, **93** (2012) 215.